THE JOURNAL OF PHYSICAL CHEMISTRY B

Article

Cite This: J. Phys. Chem. B 2019, 123, 2147−2156

pubs.acs.org/JPCB

Vibrational Optical Activity of Intermolecular, Overtone, and Combination Bands: 2-Chloropropionitrile and α-Pinene

Pavel Michal,*[,†] Radek Čelechovský,[†] Michal Dudka,[†] Josef Kapitán,[†] Milan Vůjtek,[†] Marie Berešová,[‡,§] Jaroslav Šebestík,[§] Karthick Thangavel,[§] and Petr Bouř*[,‡,§]

[†]Department of Optics, Palacký University Olomouc, 17. listopadu 12, 77146 Olomouc, Czech Republic

[‡]Department of Analytical Chemistry, University of Chemistry and Technology, Technická 5, 16628 Prague, Czech Republic

[§]Institute of Organic Chemistry and Biochemistry, Academy of Sciences, Flemingovo náměstí 2, 16610 Prague, Czech Republic

Supporting Information

ABSTRACT: Spectroscopy of vibrational optical activity has been established as a powerful tool to study molecular structures and interactions. In most cases, only fundamental molecular transitions are analyzed. In the present study, we analyze a broader range of vibrational frequencies (40−4000 cm^{-1}), which could be measured on a new Raman optical activity (ROA) instrument. An unexpectedly strong vibrational Raman optical activity of 2-chloropropionitrile has been observed within the low-frequency region (40−150 cm^{-1}). On the basis of combined molecular dynamics and density functional theory simulations, it could be assigned to intermolecular vibrations. A detailed analysis also revealed connection between spectral shapes and molecular structure and flexibility, such as bending of the CCN group. At the other edge of the scale, within ∼1500−4000 cm^{-1}, for the first time, many combination and overtone ROA bands have been observed for 2-chloropropionitrile and α-pinene. These were also partially assigned, using quantum-chemical computations. The band assignment was confirmed by a comparison with Raman, absorption, and vibrational circular dichroism spectra. The measurement in the broader vibrational range thus significantly extends the information that can be obtained by optical spectroscopy, including intermolecular interactions of chiral molecules and liquids.

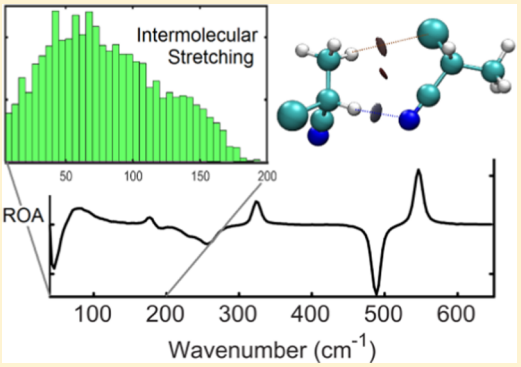

INTRODUCTION

Raman optical activity (ROA) is a quickly developing optical spectroscopic technique that explores differential scattering of left and right circularly polarized light by chiral molecules.[1,2] Similar to vibrational circular dichroism (VCD),[3] it can not only distinguish absolute configuration[4] but also provide higher structural sensitivity than that from techniques using unpolarized light. ROA bands carry information about conformational states[5] and system dynamics,[6] too. As one of rather few methods, ROA spectroscopy is applicable for molecules in solutions. It has been applied to a broad range of inorganic, organic, and biomolecules, including helicenes,[7,8] peptides,[9−11] proteins,[12,13] fibrils,[14,15] sugars,[16,17] nucleic acids,[18] and even to whole viruses.[19,20]

In the past, ROA spectra have been almost exclusively analyzed with a limited spectral range. For example, the commercial ROA spectrometer of Biotools operates within 200−2450 cm^{-1}. The range is broader than for common VCD spectrometers,[21] for example, but important parts of the spectra including hot, combination, and overtone bands are missing.

Further restrictions are imposed by difficult interpretation of the "nonstandard" spectral regions. For example, high-energy CH stretching modes (∼3000 cm^{-1}) often exhibit resonance and other effects not included in the usual harmonic approximation.[2,22−25]

In the present study, we show that some of these obstacles can be overcome. We focus on new physical insight into properties of two model molecules, which can be obtained by measurement of the low- and high-frequency bands. Raman and ROA data were recorded on a custom-built two-grid spectrometer operating within 40−3800 cm^{-1}. The instrument exhibits a large signal-to-noise ratio and a flat baseline. This makes possible the measurement of even weak overtone and combination bands, largely ignored in previous studies. ROA spectra in the high-frequency region have been reported, but they comprised fundamental transitions (CH stretching) only.[23,24]

The first molecule, 2-chloropropionitrile, is selected as a model liquid. As noticed already before,[25] it is sufficiently small to allow for precise molecular mechanics and quantum mechanics (MM/QM) computations. Surprisingly, we observed a very large ROA signal within 40−150 cm^{-1}, carrying information about intermolecular interactions. At the high-

Received: January 14, 2019
Revised: February 12, 2019
Published: February 13, 2019

DOI: 10.1021/acs.jpcb.9b00403
J. Phys. Chem. B 2019, 123, 2147−2156

frequency part of the spectrum, ROAs of overtone and combination transitions were detected. These were also obtained for α-pinene, for which the first report indicating their presence in infrared and Raman spectra appeared already in 1976,[26] followed by a series of other works.[27,28] Both molecules serve as convenient systems for testing the accuracy of contemporary computational procedures, allowing to simulate the "anharmonic" spectral features. To verify our Raman and ROA results, VCD and IR intensities are measured and compared with the simulated ones, too.

Analysis of the spectra provides interesting insight into molecular behavior. Although there is no universal way to treat the low-frequency vibrational transitions theoretically, experience shows that the conformer distribution can be obtained using methods of classical molecular mechanics (MM) and spectral properties can be calculated quantum-mechanically (QM), which is sometimes referred to as the instantaneous normal mode[29] or frozen field[30] approximation. The "multiscale" MM/QM methodology for vibrational optical activity (VOA) has been elaborated by us and other authors in the past.[31−36] Averaging of spectra from partially optimized molecular dynamics (MD) clusters takes into consideration both molecular flexibility and solvent−solute (or solvent−solvent in our case) interactions. Dielectric solvent models, such as the polarizable continuum model (PCM)[37,38] and conductor-like screening model (COSMO),[39] are used to account for longer-range solvent effects. For 2-chloropropionitrile, this procedure provided a satisfactory basis to understand the intermolecular vibrations of the liquid.

Simulations of high-frequency molecular vibrational properties in general require treatment beyond the harmonic approximation. This is a very difficult problem, accurately solvable only for simple molecules.[40−45] Fortunately, for semirigid molecules, perturbation approaches have been developed in recent years that can be applied for larger systems as well. They quite often fairly well explain the main spectral features observed experimentally below about 4000 cm^{-1}, that is, in the range of most fundamental transitions.[46,47] Obviously, they do not always provide a band-to-band correspondence to the experiment and are not usable for higher excitations. However, for the molecules studied here, a second-order perturbation approach reproduced the most prominent anharmonic features and made it possible to link observed spectral shapes to the structure.

We find these observations also useful for future developments of vibrational optical activity (VOA) spectroscopy, in particular Raman optical activity. The wavenumber extension allows for better exploitations of the information available in the vibrational spectra. In particular, the extreme chirality observed for the lowest-frequency intermolecular modes of 2-chloropropionitrile suggests that the ROA methodology may become a useful tool to study solvent−solute and other weak interactions of chiral molecules, similar to, for example, the terahertz spectroscopy.[48]

METHODS

Chemicals. Both enantiomers of α-pinene were purchased from Sigma-Aldrich; (*R*)- and (*S*)-2-chloropropionitrile (Figure 1) were prepared by a modified four-step synthesis described elsewhere.[25] Briefly, L and D-alanine were converted to (*S*)- and (*R*)-2-chloropropanoic acids, respectively.[49] Then, the acids were converted to (*S*)- and (*R*)-ethyl-2-chloropropionate by azeotropic esterification, using a mixture of benzene/ethanol and a small amount of sulfuric acid. The following reaction of the ester with cooled aqueous ammonia solution led to (*S*)- or (*R*)-2-chloropropionamide.[50] Final dehydration of the amide with P_4O_{10} provided the desired (*R*/*S*)-2-chloropropionitriles. This reaction was carried out as a bulb-to-bulb distillation using a Kugelrohr apparatus at 220 °C (8 Torr), and the product was rapidly cooled down. (*S*)-2-Chloropropionitrile: overall yield 13%. ^{1}H NMR (400 MHz, DMSO-d_6) δ 5.27 (q, *J* = 7.0 Hz, 1H, CHCl), 1.77 (d, *J* = 7.0 Hz, 3H, CH_3). ^{13}C NMR (100 MHz, DMSO) δ 118.84 (CN), 38.70 (CHCl), 22.81 (CH_3). EI-HRMS (*m*/*z*): For M^+ C_3H_4NCl calcd 89.0032, found 89.0028 (−4.5 ppm). (*R*)-2-Chloropropionitrile: overall yield 13%. ^{1}H NMR (400 MHz, DMSO-d_6) δ 5.27 (q, *J* = 7.0 Hz, 1H, CHCl), 1.77 (d, *J* = 7.0 Hz, 3H, CH_3). ^{13}C NMR (100 MHz, DMSO) δ 118.83 (CN), 38.69 (CHCl), 22.81 (CH_3). EI-HRMS (*m*/*z*): for M^+ C_3H_4NCl calcd 89.0032, found 89.0031 (−1.1 ppm).

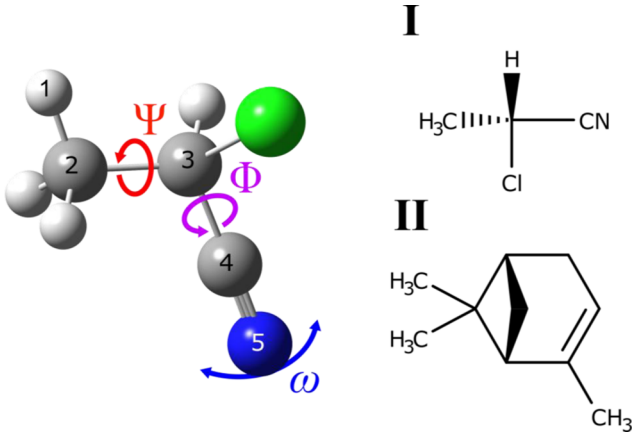

Figure 1. Studied molecules: (*R*)-2-chloropropionitrile ("nitrile", **I**) and (+)(1*R*,5*R*)-α-pinene ("α-pinene", **II**). On the left, characteristic coordinates in **I** are defined Ψ = ∠(1,2,3,4), Φ = ∠(2,3,4,5), and ω = ∠(3,4,5).

Spectra Measurement. Raman and ROA spectra were acquired on an ROA instrument constructed at Palacký University, Olomouc, largely based on the design of Hug.[51,52] Neat-liquid chiral samples were measured in a rectangular fused silica cell of 70 μL volume at room temperature (298 K), using the back-scattering geometry, scattered circular polarization (SCP) modulation scheme, and Nd:YAG laser with 532 nm excitation wavelength. Laser powers and accumulation times are listed in Table S1. *R*-Enantiomer ROA spectra are presented as averages of both enantiomers, "(*R* − *S*)/2"; unprocessed spectra can be found in the Supporting Information (Figures S1 and S2). IR and VCD nitrile spectra were measured on a BioTools ChiralIR-2X spectrometer for neat liquid, using a BaF_2 cell, 15 μm spacer, and 4 cm^{-1} resolution. For α-pinene, the CH stretching and the rest of the anharmonic region were measured using CaF_2 cells with 6 and 50 μm spacers, respectively. Experimental Raman and ROA spectra are given as number of detected electrons per excitation energy, $e{\cdot}J^{-1}$, and IR and VCD are expressed in $L{\cdot}mol^{-1}{\cdot}cm^{-1}$.

Computations. Optimized geometries; harmonic frequencies; and IR, VCD, Raman, and ROA intensities were calculated at the B3PW91[53,54]/6-311++G** level, using the Gaussian 16[55] program. The environment was mimicked by the conductor-like screening model (COSMO) with parameters for acetonitrile (ACN, mimicking compound **I**) and

DOI: 10.1021/acs.jpcb.9b00403
J. Phys. Chem. B 2019, 123, 2147−2156

cyclohexane (in the case of **II**).[39,56,57] Alternatively, the default Gaussian polarizable continuum model (PCM)[37] was used, which gave, however, very similar results, and is not discussed further. Presented spectra are Boltzmann-corrected to account for hot transitions in the lowest wavenumber region[58] and are given in arbitrary units (see also below, eq 5).

To understand the low-frequency vibrations of the nitrile, we calculated the dependence of its energy on the Ψ, Φ, and ω angles (see Figure 1 for their definition). The methyl group (Ψ) was rotated by 2.5° increments, within 0−120°, and 49 Φ and ω combinations were created so that the resultant nitrogen positions were evenly distributed on a sphere around C4 (ref 59, 155° < ω < 180°).

For liquid nitrile, molecular dynamics (MD) simulations were performed within Tinker software,[60] using the OPLSAA force field,[61] periodic boundary conditions, cubic box (16.9 Å per side), production run of 1 ns, 1 fs integration time, NVT ensemble, and temperature of 298 K. From the snapshots saved each 5 ps, 200 clusters were created, consisting of 12−19 nitrile molecules closer than 5 Å to a central one. The cluster geometries were partially optimized by the normal mode optimization procedure[62,63] as implemented in the Qgrad[64] program. In the optimization algorithm, apart from using a constant value,[36] the frequency cutoff limit was also distributed within 50−700 cm^{-1} (using a product of random and exponential functions, cf. Figure S3), which provided somewhat more realistic bandshapes. The B3PW91/6-31G*/COSMO(ACN) computational level with Grimme's dispersion correction with Becke−Johnson damping (GD3BJ)[65,66] was used for the quantum chemistry.

Modes with a significant amount of the intermolecular interactions were identified using the potential energy distribution (PED).[67] Same as for groups within one molecule,[68] six coordinates defining the molecular positions were defined (Figure 2), and PED was calculated by our Fortran programs.

Intermolecular interactions in nitrile were also inspected using the quantum topological atom-in-molecule (AIM) analysis. For 14 randomly selected dimers, noncovalent interactions were recognized as saddle points of electron density in space.[69−72]

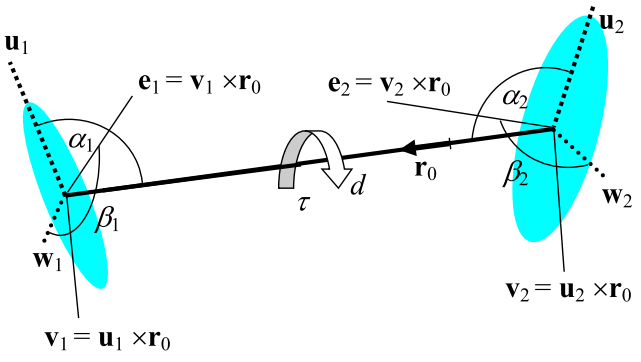

Figure 2. Definition of the six coordinates used for characterization of intermolecular vibrational modes: d, distance of the mass centers; α_1 and α_2, angles between the largest moments of inertia and the distance vector; β_1 and β_2, rotation angles; and τ, the torsion angle. For the rotation angles, arbitrary vectors $\mathbf{e}_1$ and $\mathbf{e}_1$ were defined, using the largest (direction $\mathbf{u}_i$) and second largest ($\mathbf{w}_i$) moments of inertia. Lengths of all vectors $\mathbf{u}_i$, $\mathbf{w}_i$, $\mathbf{v}_i$, $\mathbf{e}_i$, $\mathbf{r}_i$, and $\mathbf{r}_0$ are equal to 1.

Anharmonic constants (third and fourth energy derivatives, second dipole moment, and polarizability derivatives) were obtained using the Gaussian 16 and S4[73] programs at the same approximation level as for the harmonic ones. For Gaussian, two-point numerical differentiation with a step of 0.01 Å was used (steps 0.001−0.08 Å led to similar results, Figure S4). For the S4 program, a variable normal mode step was used, $q \cdot 1000 \cdot \nu^{1/2}$, where ν is the frequency in cm^{-1} and q = 0.05 Å.

The usual Taylor-expanded nuclear vibrational potential V was used as[46,74]

$$V(Q_1, ..., Q_N) = \frac{1}{2}\sum_{i=1}^{N} \nu_i^2 Q_i^2 + \frac{1}{6}\sum_{i=1}^{N}\sum_{j=1}^{N}\sum_{k=1}^{N} c_{ijk} Q_i Q_j Q_k + \frac{1}{24}\sum_{i=1}^{N}\sum_{j=1}^{N}\sum_{k=1}^{N}\sum_{l=1}^{N} d_{ijkl} Q_i Q_j Q_k Q_l \quad (1)$$

where Q_i's are the normal mode coordinates, ν_i's are the harmonic frequencies, N is the number of normal modes, c_{ijk}'s are the cubic constants, and d_{ijkl}'s are the quartic constants. Quartic constants where all indices are unique were neglected.

Using the potential (eq 1), anharmonic vibrational energies and spectral intensities were calculated using the second-order vibrational perturbation approach (VPT2)[46,74] and its modification (GVPT2) better treating the Fermi and Darling−Dennison resonances[75] as implemented in Gaussian. Alternatively, limited vibrational configuration interaction (LVCI) was applied as described in refs 46 and 23 using our S4 software.

Same as for the potential, Raman and ROA polarizabilities (α, G', and A)[74] and electric dipole moment (μ) were considered as Taylor expansions

$$X(Q, P) = X(0) + \sum_{i=1}^{N} \frac{\partial X}{\partial Q_i} Q_i + \frac{1}{2}\sum_{j=1}^{N}\sum_{i=1}^{N} \frac{\partial^2 X}{\partial Q_i \partial Q_j} Q_i Q_j + \frac{1}{6}\sum_{i=1}^{N}\sum_{j=1}^{N}\sum_{k=1}^{N} \frac{\partial^3 X}{\partial Q_i \partial Q_j \partial Q_k} Q_i Q_j Q_k \quad (2)$$

where $X(0)$ is the equilibrium value of each electromagnetic tensor. For the magnetic moment m, the expansion is slightly different[47,76,77]

$$m(Q, P) = \hbar\sum_{i=1}^{N} \frac{\partial m}{\partial P_i} P_i + \hbar\sum_{j=1}^{N}\sum_{i=1}^{N} \frac{\partial^2 m}{\partial P_i \partial Q_j} P_i Q_j + \frac{\hbar}{2}\sum_{i=1}^{N}\sum_{j=1}^{N}\sum_{k=1}^{N} \frac{\partial^3 m}{\partial P_i \partial Q_j \partial Q_k} P_i Q_j Q_k \quad (3)$$

where $\hbar$ is the reduced Planck constant and P_i is the normal mode momentum associated with Q_i.

From the polarizabilities, Raman and SCP ROA intensities for each transition i were calculated as[1]

$$I_{i,\mathrm{Raman}} = 6\sum_{\beta=1}^{3}\sum_{\alpha=1}^{3} (\alpha_{i,\alpha\alpha}\alpha_{i,\beta\beta} + 7\alpha_{i,\alpha\beta}\alpha_{i,\alpha\beta}) \quad (4a)$$

DOI: 10.1021/acs.jpcb.9b00403
J. Phys. Chem. B 2019, 123, 2147−2156

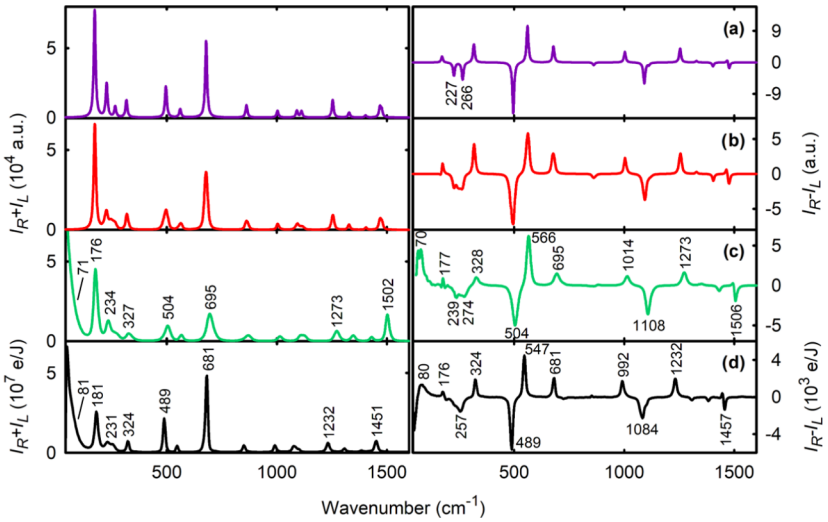

Figure 3. Raman and ROA (*R*)-2-chloropropionitrile spectra calculated for the lowest-energy conformer (a), Boltzmann average of selected density functional theory (DFT) conformers (b), and average of clusters obtained from molecular dynamics (c) and experiment (d, pure liquid).

$$I_{i,\mathrm{ROA}} = 48\sum_{\beta=1}^{3}\sum_{\alpha=1}^{3}\left(3\alpha_{i,\alpha\beta}G'_{i,\beta\alpha} - \alpha_{i,\alpha\alpha}G'_{i,\beta\beta} + \sum_{\varepsilon=1}^{3}\sum_{\gamma=1}^{3}\varepsilon_{\alpha\beta\gamma}\alpha_{i,\alpha\varepsilon}A_{i,\beta\gamma\varepsilon}\right) \quad (4b)$$

where $\alpha_i = \langle 0|\alpha|i\rangle$ (similarly for G' and A) and $|0\rangle$ and $|i\rangle$ are the ground and excited vibrational states, respectively. From these line intensities (in atomic units), theoretical spectra $S(\nu)$ dependent continuously on the frequency ν were generated using convolution with a Lorentzian function and multiplication by a Boltzmann factor

$$S(\nu) = \sum_i I_i\left[1 - \exp\left(-\frac{\nu_i}{kT}\right)\right]^{-1}\left[4\left(\frac{\nu-\nu_i}{\Delta}\right)^2 + 1\right]^{-1} \quad (5)$$

where ν_i is the transition frequency, k is the Boltzmann constant, T is the temperature, and the full width at half-maximum Δ = 10 cm^{-1}. Note that the Boltzmann factor is exactly valid for the harmonic approximation only.[58] Also, if polarizability derivatives are used instead of the transition polarizabilities, as is the case of Gaussian output, a prefactor ($\frac{1}{\nu_i}$ in the harmonic limit) must be added to eq 5.

Absorption and VCD intensities were obtained from the dipole D_i and rotational strength R_i,[1] respectively

$$D_i = \sum_{\alpha=1}^{3}\langle 0|\mu_\alpha|i\rangle\langle i|\mu_\alpha|0\rangle \quad (6a)$$

$$R_i = \mathrm{Im}\left(\sum_{\alpha=1}^{3}\langle 0|\mu_\alpha|i\rangle\langle i|m_\alpha|0\rangle\right) \quad (6b)$$

as

$$\varepsilon(\nu) = \frac{435}{4\pi}\frac{2\nu}{\Delta}\sum_i D_i\left[4\left(\frac{\nu-\nu_i}{\Delta}\right)^2 + 1\right]^{-1} \quad (7a)$$

$$\Delta\varepsilon(\nu) = \frac{435}{\pi}\frac{2\nu}{\Delta}\sum_i R_i\left[4\left(\frac{\nu-\nu_i}{\Delta}\right)^2 + 1\right]^{-1} \quad (7b)$$

where $\varepsilon/\Delta\varepsilon$ are in L·mol^{-1}·cm^{-1} and D_i/R_i are in debye^2.[78]

Minor variation of computational parameters (basis sets, functionals, omission of low-energy vibrations; see Figure S5) did not lead to significantly different results.

RESULTS AND DISCUSSION

Low-Frequency Vibrations of (*R*)-2-Chloropropionitrile Liquid. The calculated and experimental Raman and ROA spectra are presented in Figure 3. The single-conformer computation (Figure 3a) reasonably well approximates the experimental Raman and ROA intensities within ~175−1600 cm^{-1}. Nevertheless, within 176−324 cm^{-1}, we can see a significant improvement when the Boltzmann-averaged spectra are used (for one molecule, Figure 3b), using the scans over the Ψ, Φ, and ω angles. Detailed dependence of energy, geometry, and spectral parameters on these coordinates can also be seen in Figures S6−S10. Indeed, as follows from the mode assignment in Table S2 (fundamental) and Table S3 (combinations and overtones), these three coordinates to a large extent participate in the six lowest-frequency vibrations, calculated within ~170−570 cm^{-1}. Thus, for example, the two negative ROA peaks calculated for the equilibrium structure at 227 and 266 cm^{-1} become broader and merge into a broad negative signal, i.e., closer to the experimental shape (Figure 3d).

The monomolecular models a−b in Figure 3, however, cannot explain the measured signal below 176 cm^{-1}. The experimental Raman intensity rises sharply as the frequency goes to zero, almost monotonically, with a shoulder at 81 cm^{-1}. The ROA intensity is even more interesting, with a maximum at 80 cm^{-1}, and at about 62 cm^{-1}, changing its sign and becoming negative up to the optical filter limit (~40 cm^{-1}). This is to a large extent reproduced by the spectrum obtained as an average from the MD clusters (Figure 3c). This most advanced model also provides a broader and ROA-less intense "monomolecular" band at 695 cm^{-1} and minor changes in other parts of the spectra, suggesting a coupling of intermolecular and higher-frequency intramolecular vibrations.

The normal mode assignment is in agreement with the detailed analysis reported previously.[25] However, we would like to mention a rather unexpected flexibility of the C−C≡N

DOI: 10.1021/acs.jpcb.9b00403
J. Phys. Chem. B 2019, 123, 2147−2156

bond system, seen, for example, during visualization of the normal mode motion. Vibrational modes connected to the C−C≡N bending have relatively low harmonic frequencies (e.g., modes 173−561 cm^{-1}, Table S2). The equilibrium angle is calculated as $\omega \sim 179°$, but it can easily change. For example, a deviation of 16° requires energy of about 2 $kcal \cdot mol^{-1}$. Taking into account other degrees of freedom, the most probable value at room temperature is thus predicted as 177.4° (Figure S10).

According to AIM analysis,[69−72] the nitrile−nitrile intermolecular interactions are rather nonspecific and weak, including van der Waals dispersion and weak (aliphatic) hydrogen bonds with participation of the electronegative chlorine and nitrogen atoms (Table S4, Figure S11). Still, these forces generate intermolecular vibrational modes containing different contributions of the geometrical coordinates. The assignment to intermolecular modes is also confirmed with the ROA spectra obtained for a nitrile solution in methanol, where some low-frequency bands nearly vanish (Figure S12).

According to the potential energy distribution, the intermolecular stretching vibration (d, cf. Figure 2) is the most probable for modes around 70 cm^{-1} and the bending (α_i, β_i) and torsional (τ) intermolecular motions are dominant for even lower vibrational frequencies (Figure 4). Above about

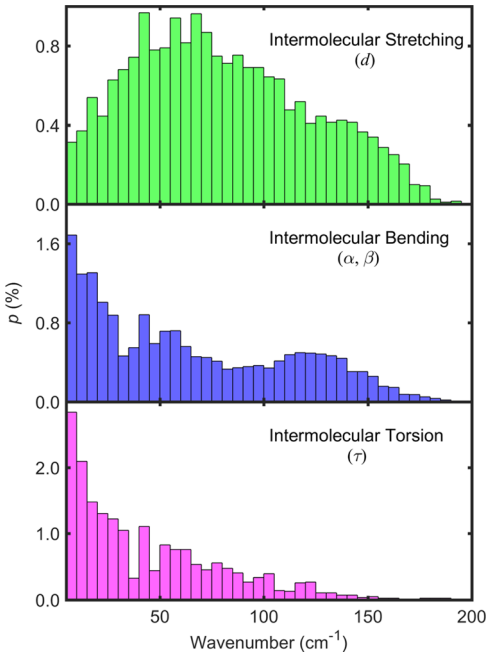

Figure 4. Relative probabilities of intermolecular coordinates (nitrile−nitrile) to the potential energy distribution, for the low-frequency modes as obtained from 200 MD clusters (a B3PW91/GD3BJ/6-31G*/COSMO(ACN) calculation).

180 cm^{-1}, the intermolecular modes vanish. Interestingly, the resultant spectra can, to a large extent, be thought of as products of dimer−dimer interactions. At least in trial computations, the ensemble of dimers obtained from the MD snapshots provided Raman and ROA shapes very similar to those obtained using the complete clusters.

To conclude this section, we could measure a strong nitrile Raman optical activity in the low-frequency region and showed that it is related to intermolecular interactions. These results suggest that the ROA spectroscopy may find new applications in studies of solvent−solute and other weak interactions including chiral discrimination. For α-pinene, a large monosign ROA (positive for the + enantiomer) close to 40 cm^{-1} is apparent as well. However, the intermolecular interactions are weaker and most of the relevant transitions probably lie under the instrumental limit.

Raman Optical Activity of Overtone and Combination Vibrations. On the other edge of the spectrum, the new ROA instrument makes it possible to record the CH stretching fundamental transitions, but also the weak overtone and combination bands. The ROA measurement of the fundamental CH vibrations has been achieved previously by a dedicated spectrometer[24] or a combination of three different interchangeable spectral gratings and intensity calibration using a fluorescence standard.[23,79] The ROA bands, however, were hampered by the strong underlying Raman scattering and were prone to instrumental artifacts. As far as we know, the overtones and combination bands have not been measured yet. In our spectrometer, the possibility to measure the extended range simultaneously is ensured by analysis of the zero-order diffraction beam by an additional spectrograph and detector. This arrangement also provides a good baseline stability and detection sensitivity.

For nitrile, the experimental and simulated Raman and ROA spectra within 1490−3800 cm^{-1} are plotted in Figure 5. As expected, the largest intensities are exhibited by the fundamental modes comprising C≡N stretching (experimentally at 2252 cm^{-1}) and CH stretching (about 3000 cm^{-1}). They are plotted within the gray areas in Figure 5. For this molecule, relative Raman and ROA intensities of the fundamental transitions seem to be fairly well modeled already at the harmonic level (the red curve), although with a huge frequency error of about 104 and 136 cm^{-1} for CN and CH stretching, respectively. Both the VPT2 and LVCI anharmonic methods correct it and provide nearly the experimental CH stretching frequencies. For the C≡N band, however, a significant energy error of 73 cm^{-1} remains even after the anharmonic corrections (cf. also Table S2). On the basis of benchmark computations (CCSD(T), MP4) on smaller model systems containing the triple bond, we can relate the remaining deviation to an inherent inaccuracy of the B3PW91 and similar functionals.

As discussed previously, the approximate anharmonic approaches comprise many simplifications and may themselves introduce errors comparable with the actual corrections.[46,75] For example, because the four lowest-frequency modes had to be omitted from the LVCI computation, resultant intensities above 3100 cm^{-1} are significantly underestimated. Below 3100 cm^{-1}, the VPT2 and LVCI methods provide similar Raman shapes, whereas for ROA, the VPT2 simulation looks more realistic when compared with experiment. Overall, the VPT2 procedure appears more practical than LVCI in this case. Based on VPT2, many combination and overtone bands can be unambiguously assigned (Figure 5 and Table S3). It is interesting that the technically more advanced generalized VPT2 variant (GVPT2), which includes corrections to Fermi and Darling−Dennison resonances, does not perform so well, although the differences are mostly minor (Figure S5). From the similarity of LVCI and VPT2 simulations, we can deduce that double-excited overtone and combination transitions involved in VTP2 are dominating, whereas contributions of higher excitations are much smaller. Higher excitations are

DOI: 10.1021/acs.jpcb.9b00403
J. Phys. Chem. B 2019, 123, 2147−2156

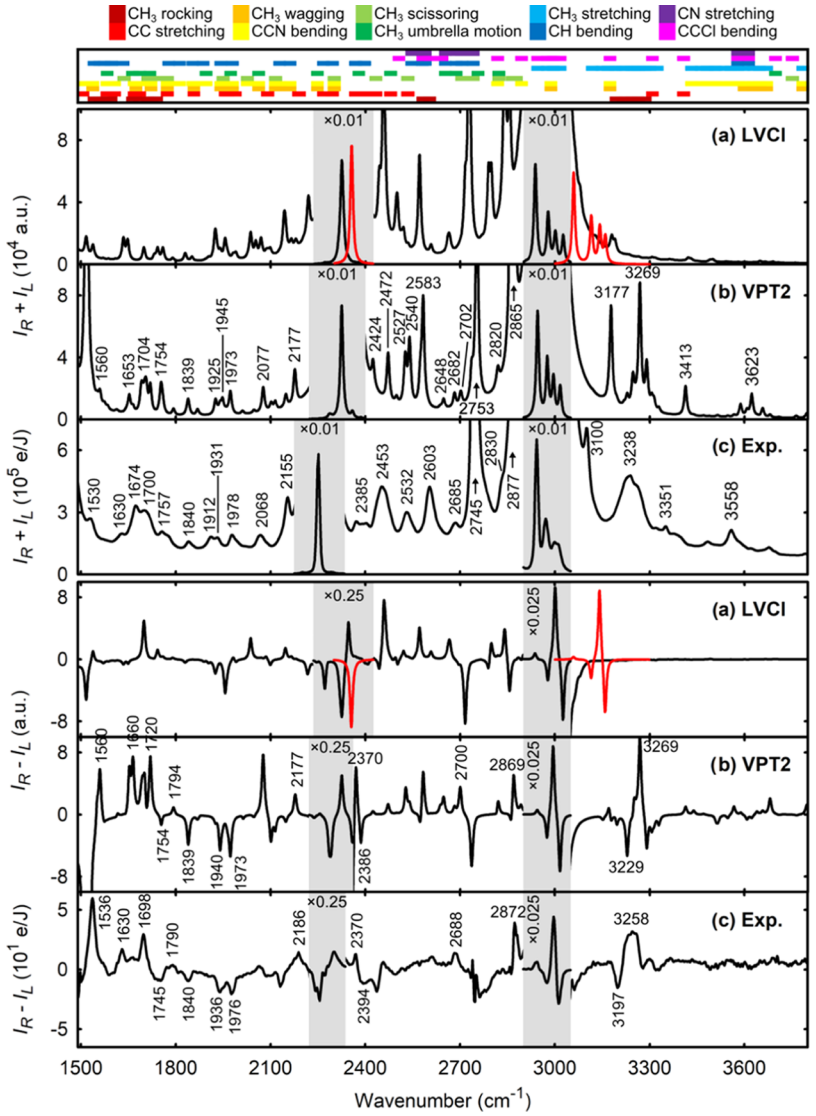

Figure 5. Raman and ROA spectra of the nitrile, plotted within 1490−3800 cm^{-1}, as calculated using the limited vibrational configuration interaction (a), vibrational second-order perturbation calculus (b), and the experiment (c). For the fundamental C≡N and CH stretching signals, spectral shapes calculated at the harmonic level are plotted by the red line. Spectral parts in the gray areas are plotted in a different scale. At the top, main coordinate contributions to the overtone and combination bands are indicated (see also Tables S2−S3).

included in the LVCI approach only, up to five times excited modes.

Same as for the fundamental modes, overtone and combination bands can also be vaguely related to chemical groups, as indicated at the very top of Figure 5. For example, within 1500−2220 cm^{-1}, CH_3 rocking and CC stretching seem to generate most of the spectral intensities. In wavenumber regions closer to the fundamental CH stretching bands (2600−2900 cm^{-1}), the CH bending modes, such as the CH_3 umbrella or CH_3 scissoring, contribute more. Below 1950 cm^{-1}, more diverse patterns take place, including CC stretching, CH_3 wagging, CCN bending, CH_3 scissoring, and CH bending. Above 3000 cm^{-1}, higher-energy fundamental modes, such as C≡N stretching, contribute more. Also, the lower-frequency fundamental motions can combine with the CH stretch.

The assignment based on the Raman and ROA bands can be confirmed by a comparison of computed and experimental IR and VCD spectra (Figure S13). The experimental VCD is somewhat hampered by the noise, in particular, above 3000 cm^{-1}. It is interesting that, contrary to the Raman and ROA bands, the C≡N stretching IR and VCD intensities (exp. 2252 cm^{-1}) are significantly overestimated by the simulations.

Analogously as for the nitrile in Figure 5, Raman and ROA spectra of α-pinene with the emphasis on the overtone and combination bands are plotted in Figure 6. Compared with the nitrile, we see several differences. As discussed previously,[23] the harmonic calculus is not adequate to reproduce the fundamental CH stretching intensity of α-pinene (~2750−3050 cm^{-1}). In addition, the bare VPT2 theory (Figure 6a) failed for the entire spectral region. This can be explained by the greater number of resonances in the molecule, which causes a divergence of the VPT2 results. Also, the LVCI method (Figure S14) did not reproduce the anharmonic region well, in spite of the extensive computational time required. Fortunately, the general GVPT2 approach (Figure 6b) gives a very good agreement with the experimental Raman and ROA spectra. Within 1800−2800 cm^{-1}, for example, the GVPT2 simulation sometimes almost amazingly faithfully reproduces the complicated ROA experimental pattern. The VOA spectroscopy combined with the theory can thus well

DOI: 10.1021/acs.jpcb.9b00403
J. Phys. Chem. B 2019, 123, 2147−2156

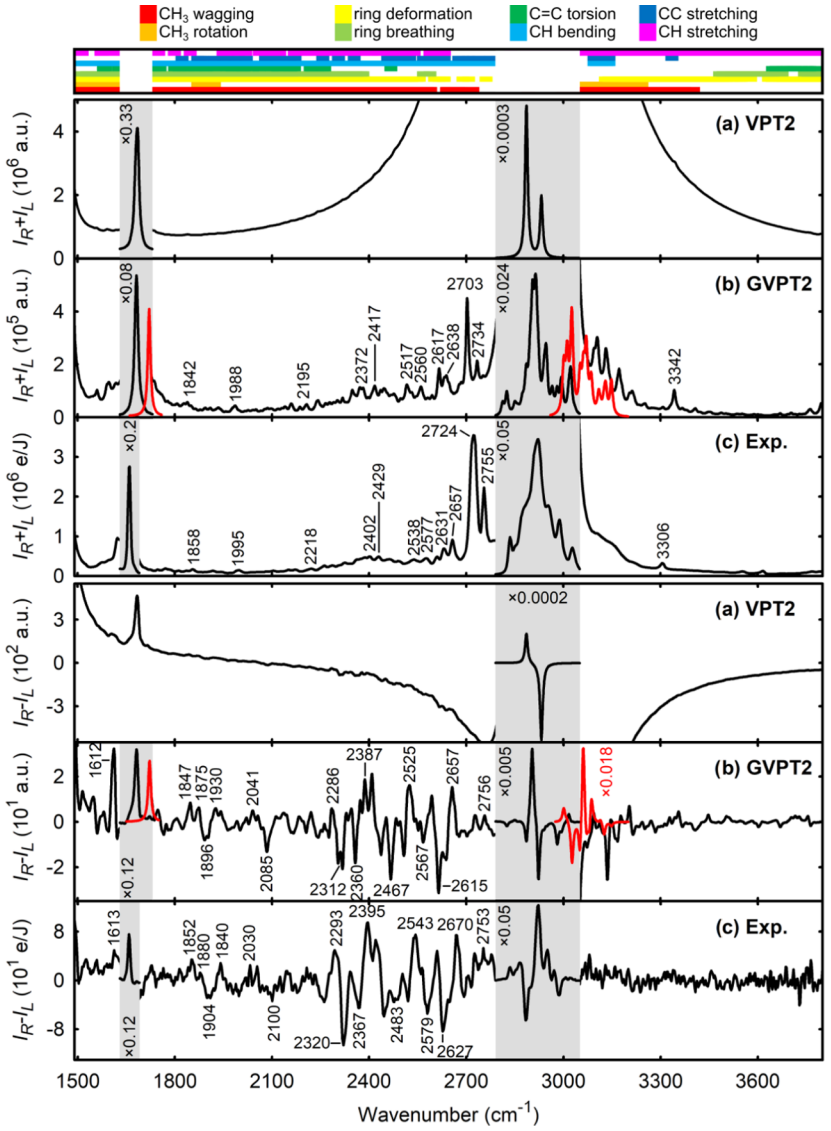

Figure 6. (+)-α-Pinene Raman and ROA spectra within 1490−3800 cm^{-1} calculated using vibrational second-order perturbation without (a) and with (b) the degeneracy correction and experiment (c). The signal of the fundamental C═C and CH stretching bands calculated at the harmonic level is plotted by the red line. At the top, main coordinate contributions to the overtone and combination bands are indicated (for vibrational normal mode assignment, see also refs 26 and 82).

complement, for example, the overtone and combination vibrational band assignments based on the isotope editing[27] or vibrational sum frequency generation studies.[80,81]

Still, inconsistencies between the simulation and experiment are apparent even for GVPT2. Relative ROA intensities of fundamental CH stretching bands are not much improved when compared with the harmonic approximation, while they grew about 3 times (cf. the multiplication factors in Figure 6). Such intensity over-estimation was not observed for LVCI (Figure S14) and can be attributed to the arbitrary wave function normalization utilized in GVPT2. The theoretical and experimental IR and VCD spectra (Figure S15) confirm that the assignment and performance of the theoretical methods are same as for the Raman and ROA data.

CONCLUSIONS

On the two model molecules, we analyzed Raman and ROA spectra obtained within the extended wavenumber range of 40−3800 cm^{-1}. The measurement was made possible by using a new spectrometer based on two detection channels. For the low-frequency region (40−150 cm^{-1}), we observed a strong optical activity of 2-chloropropionitrile that could be assigned to intermolecular vibrations. This rather surprising result suggests that the ROA spectroscopy can provide valuable information on interactions of chiral molecules and documents the convenience of chiral spectroscopy against unpolarized techniques. The underlying Raman signal was much less structured. To decipher the signal, relatively complex molecular mechanics/quantum mechanics computations were necessary, which, however, are possible with contemporary computational techniques and programs.

For the first time, we could also observe a large set of overtone and combination ROA bands in the nitrile and α-pinene spectra, mostly within 1490−3800 cm^{-1}. The experimental Raman and ROA intensities could be compared with experimental IR and VCD intensities. On the basis of the simulated spectra obtained by various perturbation and variational approaches, most intense bands could be

DOI: 10.1021/acs.jpcb.9b00403
J. Phys. Chem. B 2019, 123, 2147−2156

unambiguously assigned to double-excited overtone or double-excited combination transitions.

We thus hope that the presented results will stimulate further development of the ROA and VCD spectroscopies as incisive probes of molecular structure and behavior.

■ ASSOCIATED CONTENT

Supporting Information

The Supporting Information is available free of charge on the ACS Publications website at DOI: 10.1021/acs.jpcb.9b00403.

Computational details and tests and complementary experimental data including unprocessed nitrile and α-pinene vibrational spectra; dependence of the anharmonic force constants on differentiation step; nitrile Raman and ROA spectra calculated with various harmonic methods; energy and frequency shifts as a function of Ψ and ω; IR and VCD spectra of nitrile and α-pinene, LVCI Raman and ROA spectra of α-pinene, and AIM topological parameters of interacting atoms (PDF)

■ AUTHOR INFORMATION

Corresponding Authors

*E-mail: michal@optics.upol.cz (P.M.).
*E-mail: bour@uochb.cas.cz (P.B.).

ORCID

Pavel Michal: 0000-0002-7648-6006
Josef Kapitán: 0000-0002-1916-9186
Jaroslav Šebestík: 0000-0002-0614-2064
Petr Bouř: 0000-0001-8469-1686

Notes

The authors declare no competing financial interest.

■ ACKNOWLEDGMENTS

The work was supported by the Czech Grant Agency (17-00121S, 18-05770S), Ministry of Education (LTC17012), and computational grants of CESNET (LM2015042) and the CERIT-SC (LM2015085).

■ REFERENCES

(1) Nafie, L. A. *Vibrational Optical Activity: Principles and Applications*; Wiley, 2011.
(2) Polavarapu, P. L. *Chiroptical Spectroscopy: Fundamentals and Applications*; Taylor & Francis, 2016.
(3) Barron, L. D. *Molecular Light Scattering and Optical Activity*, 2nd ed.; Cambridge University Press: Cambridge, 2004.
(4) Haesler, J.; Schindelholz, I.; Riguet, E.; Bochet, C. G.; Hug, W. Absolute Configuration of Chirally Deuterated Neopentane. *Nature* **2007**, *446*, 526−529.
(5) Kessler, J.; Andrushchenko, V.; Kapitán, J.; Bouř, P. Insight into Vibrational Circular Dichroism of Proteins by Density Functional Modeling. *Phys. Chem. Chem. Phys.* **2018**, *20*, 4926−4935.
(6) Kapitán, J.; Baumruk, V.; Kopecký, V., Jr.; Bouř, P. Conformational Flexibility of L-Alanine Zwitterion Determines Shapes of Raman and Raman Optical Activity Spectral Bands. *J. Phys. Chem. A* **2006**, *110*, 4689−4696.
(7) Johannessen, C.; Blanch, E. W.; Villani, C.; Abbate, S.; Longhi, G.; Agarwal, N. R.; Tommasini, M.; Lightner, D. A. Raman and ROA Spectra of (−)- and (+)-2-Br-Hexahelicene: Experimental and DFT Studies of a π-Conjugated Chiral System. *J. Phys. Chem. B* **2013**, *117*, 2221−2230.
(8) Shen, C.; Srebro-Hooper, M.; Weymuth, T.; Krausbeck, F.; Navarrete, J. T. L.; Ramírez, F. J.; Nieto-Ortega, B.; Casado, J.; Reiher, M.; Autschbach, J.; et al. Redox-Active Chiroptical Switching in Mono- and Bis-Iron Ethynylcarbo[6]Helicenes Studied by Electronic and Vibrational Circular Dichroism and Resonance Raman Optical Activity. *Chem. - Eur. J.* **2018**, *24*, 15067−15079.
(9) Zhu, F.; Isaacs, N. W.; Hecht, L.; Barron, L. D. Polypeptide and Carbohydrate Structure of an Intact Glycoprotein from Raman Optical Activity. *J. Am. Chem. Soc.* **2005**, *127*, 6142−6143.
(10) Kapitán, J.; Baumruk, V.; Bouř, P. Demonstration of the Ring Conformation in Polyproline by the Raman Optical Activity. *J. Am. Chem. Soc.* **2006**, *128*, 2438−2443.
(11) Mensch, C.; Barron, L. D.; Johannessen, C. Ramachandran Mapping of Peptide Conformation Using a Large Database of Computed Raman and Raman Optical Activity Spectra. *Phys. Chem. Chem. Phys.* **2016**, *18*, 31757−31768.
(12) Barron, L. D.; Blanch, E. W.; Hecht, L. Unfolded Proteins Studied by Raman Optical Activity. In *Advances in Protein Chemistry*; Academic Press, 2002; Vol. *62*, pp 51−90.
(13) Syme, C. D.; Blanch Ewan, W.; Holt, C.; Jakes, R.; Goedert, M.; Hecht, L.; Barron Laurence, D. A Raman Optical Activity Study of Rheomorphism in Caseins, Synucleins and Tau. *Eur. J. Biochem.* **2002**, *269*, 148−156.
(14) Kessler, J.; Keiderling, T. A.; Bouř, P. Arrangement of Fibril Side Chains Studied by Molecular Dynamics and Simulated Infrared and Vibrational Circular Dichroism Spectra. *J. Phys. Chem. B* **2014**, *118*, 6937−6945.
(15) Kessler, J.; Yamamoto, S.; Bouř, P. Establishing the Link between Fibril Formation and Raman Optical Activity Spectra of Insulin. *Phys. Chem. Chem. Phys.* **2017**, *19*, 13614−13621.
(16) Šugar, J.; Bouř, P. Quantitative Analysis of Sugar Composition in Honey Using 532-nm Excitation Raman and Raman Optical Activity Spectra. *J. Raman Spectrosc.* **2016**, *47*, 1298−1303.
(17) Wu, T.; Průša, J.; Kessler, J.; Dračínský, M.; Valenta, J.; Bouř, P. Detection of Sugars Via Chirality Induced in Europium(III) Compounds. *Anal. Chem.* **2016**, *88*, 8878−8885.
(18) Barron, L. D.; Hecht, L.; Blanch, E. W.; Bell, A. F. Solution Structure and Dynamics of Biomolecules from Raman Optical Activity. *Prog. Biophys. Mol. Biol.* **2000**, *73*, 1−49.
(19) Blanch, E. W.; McColl, I. H.; Hecht, L.; Nielsen, K.; Barron, L. D. Structural Characterization of Proteins and Viruses Using Raman Optical Activity. *Vib. Spectrosc.* **2004**, *35*, 87−92.
(20) Hobro, A. J.; Rouhi, M.; Conn, G. L.; Blanch, E. W. Raman and Raman Optical Activity (ROA) Analysis of RNA Structural Motifs. *Vib. Spectrosc.* **2008**, *48*, 37−43.
(21) Keiderling, T. A. Vibrational Circular Dichroism. Comparison of Technique and Practical Considerations. In *Practical Fourier Transform Infrared Spectroscopy*; Krishnan, K., Ferraro, J. R., Eds.; Academic Press: San Diego, 1990; pp 203−284.
(22) Paterlini, M. G.; Freedman, T. B.; Nafie, L. A. Ring Current Enhanced Vibrational Circular Dichroism in the CH-Stretching Motion of Sugars. *J. Am. Chem. Soc.* **1986**, *108*, 1389−1397.
(23) Hudecová, J.; Profant, V.; Novotná, P.; Baumruk, V.; Urbanová, M.; Bouř, P. CH Stretching Region: Computational Modeling of Vibrational Optical Activity. *J. Chem. Theory Comput.* **2013**, *9*, 3096−3108.
(24) Hug, W.; Kint, S.; Bailey, G. F.; Schere, J. R. Raman Circular Intensity Differential Spectroscopy. The Spectra of (−)-α-Pinene and (+)-α-Phenylethylamine. *J. Am. Chem. Soc.* **1975**, *97*, 5589−5590.
(25) Wiberg, K. B.; Wang, Y.-g.; Wilson, S. M.; Vaccaro, P. H.; Cheeseman, J. R. Chiroptical Properties of 2-Chloropropionitrile. *J. Phys. Chem. A* **2005**, *109*, 3448−3453.
(26) Wilson, H. W. The Infrared and Raman Spectra of α- and β-Pinenes. *Appl. Spectrosc.* **1976**, *30*, 209−212.
(27) Upshur, M. A.; Chase, H. M.; Strick, B. F.; Ebben, C. J.; Fu, L.; Wang, H.; Thomson, R. J.; Geiger, F. M. Vibrational Mode Assignment of α-Pinene by Isotope Editing: One Down, Seventy-One to Go. *J. Phys. Chem. A* **2016**, *120*, 2684−2690.
(28) Stokes, G. Y.; Chen, E. H.; Buchbinder, A. M.; Paxton, W. F.; Keeley, A.; Geiger, F. M. Atmospheric Heterogeneous Stereochemistry. *J. Am. Chem. Soc.* **2009**, *131*, 13733−13737.

DOI: 10.1021/acs.jpcb.9b00403
J. Phys. Chem. B 2019, 123, 2147−2156

(29) Keyes, T. Instantaneous Normal Mode Approach to Liquid State Dynamics. *J. Phys. Chem. A* **1997**, *101*, 2921−2930.
(30) Ojamäe, L.; Tegenfeldt, J.; Lindgren, J.; Hermansson, K. Simulation of Band Widths in Liquid Water Spectra. The Breakdown of the Frozen-Field Approximation. *Chem. Phys. Lett.* **1992**, *195*, 97−103.
(31) Kapitán, J.; Baumruk, V.; Kopecký, V.; Pohl, R.; Bouř, P. Proline Zwitterion Dynamics in Solution, Glass, and Crystalline State. *J. Am. Chem. Soc.* **2006**, *128*, 13451−13462.
(32) Kapitán, J.; Johannessen, C.; Bouř, P.; Hecht, L.; Barron, L. D. Vibrational Raman Optical Activity of 1-Phenylethanol and 1-Phenylethylamine: Revisiting Old Friends. *Chirality* **2009**, *21*, E4−12.
(33) Hopmann, K. H.; Ruud, K.; Pecul, M.; Kudelski, A.; Dračínský, M.; Bouř, P. Explicit Versus Implicit Solvent Modeling of Raman Optical Activity Spectra. *J. Phys. Chem. B* **2011**, *115*, 4128−4137.
(34) Zielinski, F.; Mutter, S. T.; Johannessen, C.; Blanch, E. W.; Popelier, P. L. A. The Raman Optical Activity of β-D-Xylose: Where Experiment and Computation Meet. *Phys. Chem. Chem. Phys.* **2015**, *17*, 21799−21809.
(35) Cheeseman, J. R.; Shaik, M. S.; Popelier, P. L. A.; Blanch, E. W. Calculation of Raman Optical Activity Spectra of Methyl-β-D-Glucose. Incorporating a Full Molecular Dynamics Simulation of Hydration Effects. *J. Am. Chem. Soc.* **2011**, *133*, 4991−4997.
(36) Hudecová, J.; Hopmann, K. H.; Bouř, P. Correction of Vibrational Broadening in Molecular Dynamics Clusters with the Normal Mode Optimization Method. *J. Phys. Chem. B* **2012**, *116*, 336−342.
(37) Tomasi, J.; Mennucci, B.; Cammi, R. Quantum Mechanical Continuum Solvation Models. *Chem. Rev.* **2005**, *105*, 2999−3094.
(38) Cossi, M.; Scalmani, G.; Rega, N.; Barone, V. New Developments in the Polarizable Continuum Model for Quantum Mechanical and Classical Calculations on Molecules in Solution. *J. Chem. Phys.* **2002**, *117*, 43−54.
(39) Klamt, A.; Schuurmann, G. Cosmo: A New Approach to Dielectric Screening in Solvents with Explicit Expressions for the Screening Energy and Its Gradient. *J. Chem. Soc., Perkin Trans. 2* **1993**, 799−805.
(40) Cappelli, C.; Monti, S.; Scalmani, G.; Barone, V. On the Calculation of Vibrational Frequencies for Molecules in Solution Beyond the Harmonic Approximation. *J. Chem. Theory Comput.* **2010**, *6*, 1660−1669.
(41) Cappelli, C.; Bloino, J.; Lipparini, F.; Barone, V. Toward Ab Initio Anharmonic Vibrational Circular Dichroism Spectra in the Condensed Phase. *J. Phys. Chem. Lett.* **2012**, *3*, 1766−1773.
(42) Carnimeo, I.; Puzzarini, C.; Tasinato, N.; Stoppa, P.; Charmet, A. P.; Biczysko, M.; Cappelli, C.; Barone, V. Anharmonic Theoretical Simulations of Infrared Spectra of Halogenated Organic Compounds. *J. Chem. Phys.* **2013**, *139*, No. 074310.
(43) Merten, C.; Bloino, J.; Barone, V.; Xu, Y. Anharmonicity Effects in the Vibrational CD Spectra of Propylene Oxide. *J. Phys. Chem. Lett.* **2013**, *4*, 3424−3428.
(44) Barone, V.; Biczysko, M.; Bloino, J. Fully Anharmonic IR and Raman Spectra of Medium-Size Molecular Systems: Accuracy and Interpretation. *Phys. Chem. Chem. Phys.* **2014**, *16*, 1759−1787.
(45) Barone, V.; Biczysko, M.; Bloino, J.; Puzzarini, C. Accurate Molecular Structures and Infrared Spectra of Trans-2,3-Dideuteroox-irane, Methyloxirane, and Trans-2,3-Dimethyloxirane. *J. Chem. Phys.* **2014**, *141*, No. 034107.
(46) Daněček, P.; Bouř, P. Comparison of the Numerical Stability of Methods for Anharmonic Calculations of Vibrational Molecular Energies. *J. Comput. Chem.* **2007**, *28*, 1617−1624.
(47) Bloino, J.; Biczysko, M.; Barone, V. Anharmonic Effects on Vibrational Spectra Intensities: Infrared, Raman, Vibrational Circular Dichroism and Raman Optical Activity. *J. Phys. Chem. A* **2015**, *119*, 11862−11874.
(48) Mihrin, D.; Wugt Larsen, R. THz Spectroscopy of Weakly Bound Cluster Molecules in Solid Para-Hydrogen: A Sensitive Probe of van Der Waals Interactions. *Phys. Chem. Chem. Phys.* **2019**, 349−358.
(49) Koppenhoefer, B.; Schurig, V. (S)-2-Chloroalkanoic Acids of High Enantiomeric Purity from (S)-2-Amino Acids: (S)-2-Chloropropanoic Acid. *Org. Synth.* **1988**, *66*, 151.
(50) Stork, G.; Worrall, W. S.; Pappas, J. J. Synthesis and Reactions of Glycidonitriles. Transformation into α-Haloacyl Compounds and Aminoalcohols. *J. Am. Chem. Soc.* **1960**, *82*, 4315−4323.
(51) Hug, W.; Hangartner, G. A Novel High-Throughput Raman Spectrometer for Polarization Difference Measurements. *J. Raman Spectrosc.* **1999**, *30*, 841−852.
(52) Hug, W. Virtual Enantiomers as the Solutuion of Optical Activity's Deterministic Offset Problem. *Appl. Spectrosc.* **2003**, *57*, 1−13.
(53) Kohn, W.; Sham, L. J. Self-Consistent Equations Including Exchange and Correlation Effects. *Phys. Rev.* **1965**, *140*, A1133−A1138.
(54) Becke, A. D. Density Functional Thermochemistry. III. The Role of Exact Exchange. *J. Chem. Phys.* **1993**, *98*, 5648−5652.
(55) Frisch, M. J.; Trucks, G. W.; Schlegel, H. B.; Scuseria, G. E.; Robb, M. A.; Cheeseman, J. R.; Scalmani, G.; Barone, V.; Petersson, G. A.; Nakatsuji, H.;et al.et al.*Gaussian 16*, revsion A.03; Wallingford, CT, 2016.
(56) Barone, V.; Cossi, M. Quantum Calculation of Molecular Energies and Energy Gradients in Solution by a Conductor Solvent Model. *J. Phys. Chem. A* **1998**, *102*, 1995−2001.
(57) Cossi, M.; Rega, N.; Scalmani, G.; Barone, V. Energies, Structures, and Electronic Properties of Molecules in Solution with the C-PCM Solvation Model. *J. Comput. Chem.* **2003**, *24*, 669−681.
(58) Polavarapu, P. L. *Vibrational Spectra: Principles and Applications with Emphasis on Optical Activity*; Elsevier: Amsterdam, 1998; Vol. *85*.
(59) Deserno, M. *How to Generate Equidistributed Points on the Surface of a Sphere*; Max-Planck-Institut für Polymerforschung: Germany, 2004.
(60) Ponder, J. W. *Tinker, Software Tools for Molecular Design*, 7.2.1st ed.; Washington University: St. Louis, Missouri, 2000.
(61) Rizzo, R. C.; Jorgensen, W. L. OPLS All-Atom Model for Amines: Resolution of the Amine Hydration Problem. *J. Am. Chem. Soc.* **1999**, *121*, 4827−4836.
(62) Bouř, P.; Keiderling, T. A. Partial Optimization of Molecular Geometry in Normal Coordinates and Use as a Tool for Simulation of Vibrational Spectra. *J. Chem. Phys.* **2002**, *117*, 4126−4132.
(63) Bouř, P. Convergence Properties of the Normal Mode Optimization and Its Combination with Molecular Geometry Constraints. *Collect. Czech. Chem. Commun.* **2005**, *70*, 1315−1340.
(64) Bouř, P. *Qgrad*; Institute of Organic Chemistry and Biochemistry, Academy of Sciences: Prague, Czech Republic, 2006.
(65) Grimme, S.; Antony, J.; Ehrlich, S.; Krieg, H. A Consistent and Accurate Ab Initio Parametrization of Density Functional Dispersion Correction (DFT-D) for the 94 Elements H-Pu. *J. Chem. Phys.* **2010**, *132*, No. 154104.
(66) Grimme, S.; Ehrlich, S.; Goerigk, L. Effect of the Damping Function in Dispersion Corrected Density Functional Theory. *J. Comput. Chem.* **2011**, *32*, 1456−1465.
(67) Wilson, E. B. A Method of Obtaining the Expanded Secular Equation for the Vibration Frequencies of a Molecule. *J. Chem. Phys.* **1939**, *7*, 1047−1052.
(68) Hug, W.; Fedorovsky, M. Characterizing Vibrational Motion Beyond Internal Coordinates. *Theor. Chem. Acc.* **2008**, *119*, 113−131.
(69) Kumar, P. S. V.; Raghavendra, V.; Subramanian, V. Bader's Theory of Atoms in Molecules (AIM) and Its Applications to Chemical Bonding. *J. Chem. Sci.* **2016**, *128*, 1527−1536.
(70) Bader, R. F. W. A Quantum Theory of Molecular Structure and Its Applications. *Chem. Rev.* **1991**, *91*, 893−928.
(71) Johnson, E. R.; Keinan, S.; Mori-Sánchez, P.; Contreras-García, J.; Cohen, A. J.; Yang, W. Revealing Noncovalent Interactions. *J. Am. Chem. Soc.* **2010**, *132*, 6498−6506.
(72) Lu, T.; Chen, F. Multiwfn: A Multifunctional Wavefunction Analyzer. *J. Comput. Chem.* **2012**, *33*, 580−592.

DOI: 10.1021/acs.jpcb.9b00403
J. Phys. Chem. B 2019, 123, 2147−2156

(73) Bouř, P. *S4: Program for Calculation of Anharmonic Molecular Vibrational Properties*; Institute of Organic Chemistry and Biochemistry, Academy of Sciences: Prague, Czech Republic, 2017.
(74) Barone, V. Anharmonic Vibrational Properties by a Fully Automated Second-Order Perturbative Approach. *J. Chem. Phys.* **2004**, *122*, No. 014108.
(75) Bloino, J. A VPT2 Route to Near-Infrared Spectroscopy: The Role of Mechanical and Electrical Anharmonicity. *J. Phys. Chem. A* **2015**, *119*, 5269−5287.
(76) Stephens, P. J. Theory of Vibrational Circular Dichroism. *J. Phys. Chem.* **1985**, *89*, 748−752.
(77) Keiderling, T. A.; Bouř, P. Theory of Molecular Vibrational Zeeman Effects as Measured with Circular Dichroism. *Phys. Rev. Lett.* **2018**, *121*, No. 073201.
(78) Bouř, P.; McCann, J.; Wieser, H. Measurement and Calculation of Absolute Rotational Strengths for Camphor, Alpha-Pinene, and Borneol. *J. Phys. Chem. A* **1998**, *102*, 102−110.
(79) Profant, V.; Pazderková, M.; Pazderka, T.; Maloň, P.; Baumruk, V. Relative Intensity Correction of Raman Optical Activity Spectra Facilitates Extending the Spectral Region. *J. Raman Spectrosc.* **2014**, *45*, 603−609.
(80) Ho, J.; Psciuk, B. T.; Chase, H. M.; Rudshteyn, B.; Upshur, M. A.; Fu, L.; Thomson, R. J.; Wang, H.; Geiger, F. M.; Batista, V. S. Sum Frequency Generation Spectroscopy and Molecular Dynamics Simulations Reveal a Rotationally Fluid Adsorption State of α-Pinene on Silica. *J. Phys. Chem. C* **2016**, *120*, 12578−12589.
(81) Buchbinder, A. M.; Gibbs-Davis, J. M.; Stokes, G. Y.; Peterson, M. D.; Weitz, E.; Geiger, F. M. Method for Evaluating Vibrational Mode Assignments in Surface-Bound Cyclic Hydrocarbons Using Sum-Frequency Generation. *J. Phys. Chem. C* **2011**, *115*, 18284−18294.
(82) Bouř, P.; Baumruk, V.; Hanzlíková, J. Measurement and Calculation of the Raman Optical Activity of Alpha-Pinene and Trans-Pinane. *Collect. Czech. Chem. Commun.* **1997**, *62*, 1384−1395.

DOI: 10.1021/acs.jpcb.9b00403
J. Phys. Chem. B 2019, 123, 2147−2156